NJC

Accepted Manuscript

This is an *Accepted Manuscript*, which has been through the Royal Society of Chemistry peer review process and has been accepted for publication.

Accepted Manuscripts are published online shortly after acceptance, before technical editing, formatting and proof reading. Using this free service, authors can make their results available to the community, in citable form, before we publish the edited article. We will replace this *Accepted Manuscript* with the edited and formatted *Advance Article* as soon as it is available.

You can find more information about *Accepted Manuscripts* in the Information for Authors.

Please note that technical editing may introduce minor changes to the text and/or graphics, which may alter content. The journal's standard Terms & Conditions and the Ethical guidelines still apply. In no event shall the Royal Society of Chemistry be held responsible for any errors or omissions in this *Accepted Manuscript* or any consequences arising from the use of any information it contains.

ROYAL SOCIETY OF CHEMISTRY

www.rsc.org/njc

Fabrication of TiO_2/Porous Carbon Nanofibers with Superior Visible photocatalytic activity

Xin Li, Huiming Lin*, Xiang Chen, Hao Niu, Ting Zhang, Jiuyu Liu, Fengyu Qu*

College of Chemistry and Chemical Engineering, Harbin Normal University, P. R. China, Harbin 150025

Corresponding author: Tel/Fax: +86 0451 88060653.

E-mail address: qufengyu@hrbnu.edu.cn and linhuiming@hrbnu.edu.cn

Abstract

TiO_2/porous carbon nanofibers (TiO_2/PCNFs) were prepared for visible photocatalysis for dye pollution. PCNFs were synthesized via electrospinning technique, showing the numerous porous structure and large surface. After the hydrothermal treatment, TiO_2 nanorods deposit onto PCNFs to obtain TiO_2/PCNFs heterostructure. By adjusting the mount of Ti source, the mount of TiO_2 nanorods could be easily controlled. Congo red (CR), methylene blue (MB), methyl orange (MO), eosin red (ER) were adopted as the model dye molecules, and the adsorption and visible photocatalysis were carried out in detail. All TiO_2/PCNFs exhibit enhanced visible photocatalytic efficiency and good recycle ability due to the large surface, improved visible light absorption and high separation efficiency of photogenerated electron/hole. Especially, TiO_2/PCNFs-4 possesses the efficient decolored behavior to MB solution even with the high concentration (120 mg/L, 70 min), ascribing the high adsorption capacity derived from the strong electrostatic interaction and structure match between TiO_2/PCNFs-4 and MB. These TiO_2/PCNFs heterostructures exhibit the great potential practical application to eliminate the organic pollutants from wastewater.

Keywords: TiO_2/PCNFs; heterostructures; visible light; photocatalysis

1. Introduction

With the rapid progress of industry and development of society, the water pollution from the textile dyeing industry (organic dye pollution) has been getting more serious. The organic dye pollution has drawn extensive attention due to the high stability to temperature, light and many chemicals. At present, physical adsorption and photocatalytic degradation are the two main means to treat the organic dye in wastewater. Photocatalytic degradation is considered as a clean, economical, environmentally friendly "green" technique to offer great potential for complete degradation of organic dyes into pollution free.[1, 2]

In recent years, many kinds of semiconductor metal oxide, such as TiO_2, ZnO, Bi_2O_3, Fe_2O_3[3-15] and so forth, were prepared to be used as the photocatalysts to effectively treat the pollutions. As the most promising photocatalyst, TiO_2 nanomaterials has been widely applied for the degradation of organic pollutants because of its high photosensitivity, excellent chemical stability, nontoxic nature and low cost.[1, 16, 17] As is known to all, UV light is necessary for TiO_2 nanomaterial to achieve the photodegradation owing to its wide band gap (3.0 or 3.2 eV), but that becomes the main drawback of TiO_2 nanomaterial because of its limited sunlight (about 3-5 % UV light) utilization.[18-21] To improve the utilization of solar energy, many attempts have been made to extend the photo-response of TiO_2 to visible region. On account of the previous reports, TiO_2 was sensitized with many short band gap compositions or surface modification, such as doping N,[22] noble metal/TiO_2,[23-25] metal oxides,[26] sulfide/TiO_2 heterojunction[27, 28] or carbonaceous materials/TiO_2,[18, 29, 30] and

so on, to obviously improve the photocatalytic activity under solar irradiation by extending the photo-responding range and increasing the electron-hole pair separation efficiency.[31]

Among these, carbonaceous materials, including multiwalled carbon nanotubes,[32] graphene,[33-35] and activated carbon,[36] have been combined with TiO_2 to show the enhanced visible photocatalytic activity owing to the wide visible light absorption of carbonaceous component. Zhuang and coworkers[37] reported an interesting method of synthesizing the hierarchical TiO_2@C hybrid hollow sphere giving rise to enhanced photocatalytic efficiency (97%) for the visible-light photo oxidation of rhodamine B. Zhang *et al.*[38] successful fabricated TiO_2@CNFs core/shell nanofibers, exhibiting enhanced photocatalytic activity for the decomposition of RB under visible-light irradiation.

Herein, the TiO_2 combining with one-dimensional porous carbon nanofibers (TiO_2/PCNFs) heterostructures were prepared as shown in Scheme 1. First, the PCNFs were synthesized via simple electrospinning technique, showing uniform nanofibers and plenty of porous structures. And then, these PCNFs were immersed in titanium precursor solution ($TiCl_4$ and H_2O_2) under solvothermal treatment. The partial hydrolysis of the titanium precursor can lead to many -Ti-O-Ti- fractions, which would be subsequently condensed into TiO_2 nanoparticles as crystal seeds fixing on the surface of PCNFs, and then these crystal seeds further grow into nanorods structure with the extended reaction time to obtain TiO_2/PCNFs heterostructure. With numerous porous structure, there are abundant TiO_2 nanorods

depositing onto PCNFs. Considering their novel structure, the adsorption and visible photocatalytic degradation toward methylene blue (MB), Congo red (CR), eosin red (ER) and methyl orange (MO) has been investigated, showing the excellent decoloring ability even toward the high concentration dye solution.

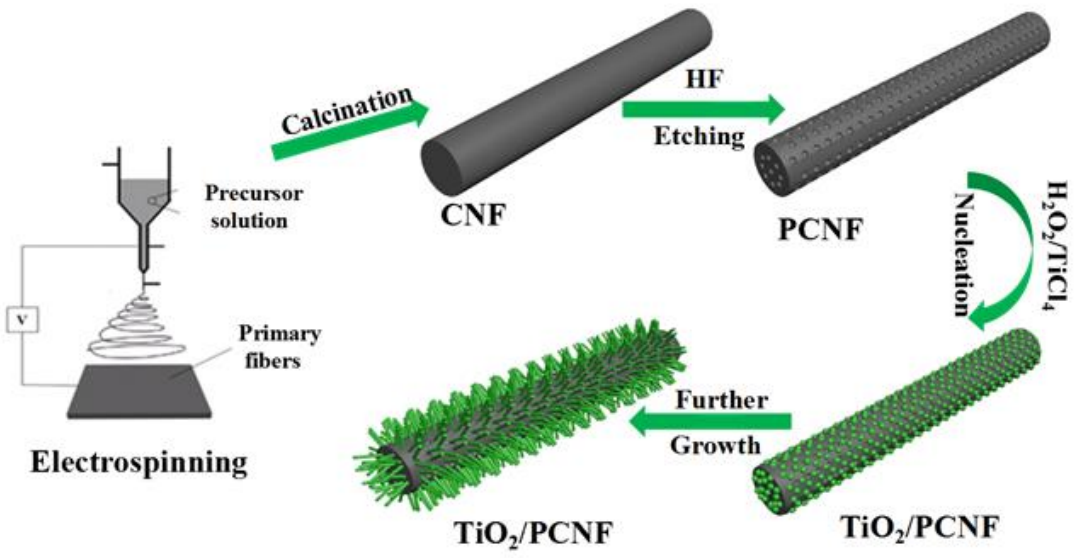

Scheme 1 The possible formation mechanism of TiO_2/PCNFs heterostructures.

2. Experimental

2.1. Materials

Triblock copolymer Pluronic P123 ($EO_{20}PO_{70}EO_{20}$, Mw = 5800), polyvinyl pyrrolidone (PVP, Mw=1, 300,000) were purchased from Aldrich Corporation. Hydrochloric acid (HCl), tetraethyl orthosilicate (TEOS), ethanol and hydrofluoric acid (HF) were bought from Tianjin Fu Yu Chemical Co.. Titanium tetrachloride ($TiCl_4$) was purchased from Aladdin (China). H_2O_2 was obtained from Tianjin Tian Li Chemical Co.. Congo red (CR), methylene blue (MB), methyl orange (MO), eosin red

(ER) were bought from Tianjin Guang Fu Chemical Co.. All the reagents were of analytical grade and used without further purification.

2.2. Synthesis of the porous carbon nanofibers (PCNFs)

In a typical experiment, P123, PVP, HCl, TEOS, and resin precursors[39] were dissolved in ethanol to form homogeneous solution and stirred for 3 h. Then, a variable high voltage power supply (Gamma FL 32174) was used to provide a high voltage (18 kV) for the electrospinning of the as-prepared solutions. Afterwards, the as-collected fibers were heated in an oven at 100 ℃ for 24 h. Then the fibers were carbonized at 800 ℃ for 4 h under N_2. Subsequently, the silica template was removed by HF treatment for 24 h. Finally, the obtained PCNFs fabrics were filtrated and washed with distilled water for several times and dried at 25 ℃.

2.3. Synthesis of TiO_2 nanorods/PCNFs heterostructures

In a typical procedure, 0.25 mL of $TiCl_4$ was dissolved in the 20 mL of H_2O_2 under magnetic stirring 2 h to become uniform solution. The resulting solution and the obtained PCNFs (3.4 mg) were transferred into a Teflon-lined stainless autoclave, sealed and maintained at 120 ℃ for 24 h. After it was cooled to room temperature, the precipitate was collected, rinsed using deionized water and finally dried at room temperature for 12 h. With different volume of $TiCl_4$ in growth solution, the resultant composites named as TiO_2/PCNFs-1 (0.05 mL), TiO_2/PCNFs-2 (0.1 mL), TiO_2/PCNFs-3 (0.2 mL), TiO_2/PCNFs-4 (0.25 mL) and TiO_2/PCNFs-5 (0.3 mL), respectively.

2.4. Photocatalytic test

The photocatalytic activity was measured by the degradation of eosin red (ER), Congo red (CR), methylene blue (MB) and methyl orange (MO), respectively. In a typical process, 0.05 g of TiO_2/PCNFs sample was suspended in 200 ml Congo red aqueous solution (10 mg/L).The suspensions were magnetically stirred 1 h in the dark to ensure adsorption/desorption equilibrium, and the solution was then exposed to a 800 W Xenon lamp. At given irradiation time intervals, the samples were collected regularly to measure the Congo red degradation by UV-Vis spectroscopy. Afterwards, the experiments of the photocatalytic degradation of eosin red aqueous solution, methylene blue and methyl orange aqueous solution were also conducted under the same conditions. After the photocatalytic test of degrading 10 mg/L MB, the TiO_2/PCNFs-4 heterostructure was then separated from the solution by centrifuging, washing clean exhaustive with ethanol to fully remove the residual organic species, then reused for the next run to test the recycle ability.

2.5. Characterization

The phase and composition of the as-obtained products were characterized by X-ray diffraction (XRD, Rigaku Dmax-rB, Cu Kα radiation, 40 KV, 100 mA). The morphology and microstructure of the samples were characterized by scanning electron microscopy (SEM, Hitachi-4800) and transmission electron microscopy (TEM, JEOL 2010EX). A specific surface area analyzer (NOVA2000E) was used to measure the N_2 adsorption/desorption. The Brunauer –Emmett–Teller (BET) formula was further used to calculate the specific surface area. The efficiency of the photocatalytic degradation was analyzed by monitoring dye decolorization at the

maximum absorption wavelength, using a UV-Vis spectrometer (Shimadzu UV-2550). UV–Vis absorption spectra of these samples were recorded at a Cary 4000 spectrophotometer in the wavelength range of 200–800 nm. Zeta potential was carried out on Zeta PALS zeta potential analyzer. Thermal gravimetry-differential thermal analysis (TG-DTA) was studied with Diamond 6300.

3. Results and discussion

The TiO_2/PCNFs heterostructures with 1D nanostructure were successfully fabricated by hydrothermal growth of TiO_2 nanorods on PCNFs. The porous structure and large surface associated with the enhanced visible absorption indicate their great potential application on wastewater decoloration.

3.1. Morphological of the as-synthesized samples studies

Morphologies and structures of TiO_2/PCNFs-4 were firstly studied by SEM and TEM as present in Fig. 1. From Fig. 1a and b, it could be clearly seen that the prepared pure PCNFs exhibit the uniform 1D fiber structure with smooth surface about several microns in length and 500-600 nm in diameter. In addition, the PCNFs interconnect with each other to form macroporous structure that benefits to the translation of the dye molecules. After the combination with TiO_2, TiO_2/PCNFs-4 still remains the fiber framework, and its surface becomes rough and flocky. From the high magnified SEM image (Fig.1d), the flocky layer is composed by the high density of secondary TiO_2 nanorods about 100-200 nm in length and 5-10 nm in diameter. In order to further investigate the microstructure of TiO_2/PCNFs-4, the TEM images are recorded as depicted in Fig.1e and f. From Fig.1e, it could be seen that a large number of TiO_2

nanorods were uniformly upright standing on the surface of PCNFs. The high resolution TEM (HRTEM) image (Fig. 1f) demonstrates the obvious lattice structure, implying the high degree of crystallinity of TiO_2. And the interplanar spacing of 0.21, 0.32 nm and 0.24 nm agrees well with the spacing of the (111), (110) lattice plane of rutile TiO_2 (R) and (004) lattice plane of anatase TiO_2 (A), respectively.

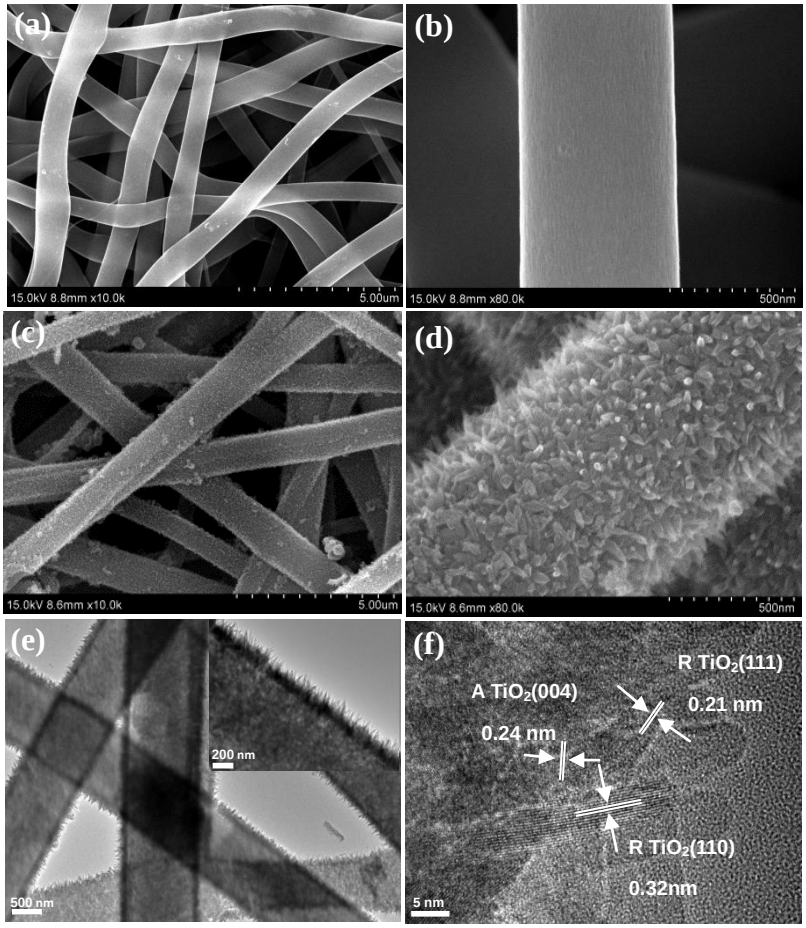

Fig. 1 SEM of the porous carbon nanofibers (a, b) and TiO_2/PCNFs-4 heterostructure (c, d). TEM images (e) and the high-resolution TEM image (f) of TiO_2/PCNFs-4.

Subsequently, by adjusting the amount of $TiCl_4$, TiO_2/PCNFs-1, TiO_2/PCNFs-2, TiO_2/PCNFs-3 and TiO_2/PCNFs-5 were prepared as exhibited in Fig. 2. From Fig.

2a-d, all samples also reveal the fiber networks combined with many TiO_2 nanorods coating on every fiber. Furthermore, the surface of the composites becomes rougher and rougher with the increase of the amount of $TiCl_4$, and there are more TiO_2 nanorods with bigger size growing on the PCNFs. As shown in Fig. 2e-h, these TiO_2 nanorods become longer and fuller depositing outside the PCNFs, processing about 100 nm in length of TiO_2/PCNFs-5 (Fig. 2h).

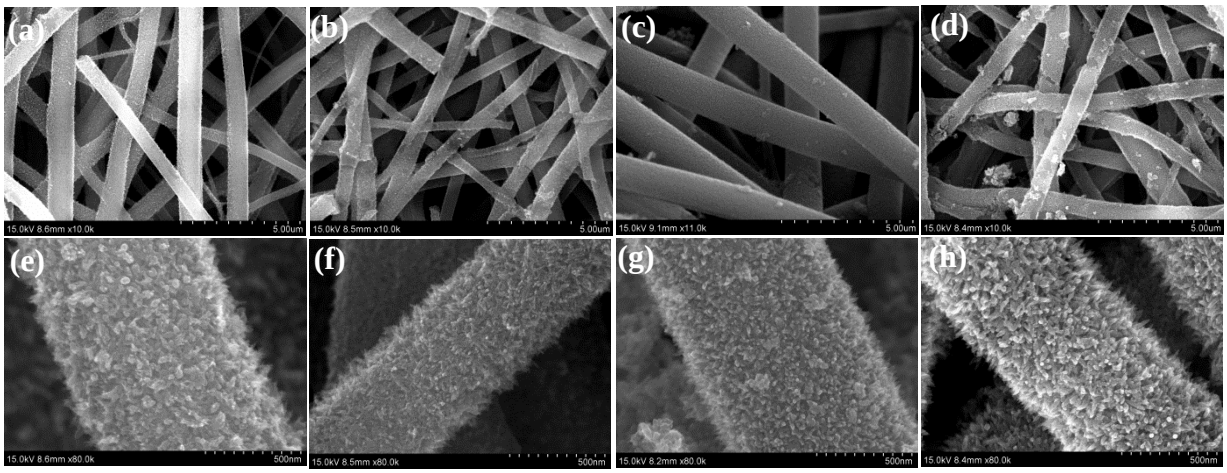

Fig. 2 SEM images of TiO_2/PCNFs-1 (a, e), TiO_2/PCNFs-2 (b, f), TiO_2/PCNFs-3 (c, g) and TiO_2/PCNFs-5 (d, h).

3.2. XRD studies

The crystallinity of the TiO_2/PCNFs heterostructures are analyzed by XRD (Fig. 3). Combining with TiO_2, the presence of typical diffraction peaks at 2θ values of 25.3, 37.8, 48.0 ,55.1 and 62.7 ° can be ascribed as the typical (101), (004), (200), (211) and (204) diffraction of anatase (A)TiO_2. There are supernumerary and visible diffraction peaks at 2θ = 27.4 and 36.1 ° agreeing well with (110) and (101) diffraction of rutile

(R) TiO_2. Based on many reports, it is reported that the coupling of anatase with rutile TiO_2 always shows an improved photocatalytic activity over anatase and rutile respectively.[31, 40] Moreover, the strongest diffraction peak of TiO_2/PCNFs-5 benefits from the highest crystallinity with the most Ti precursor.

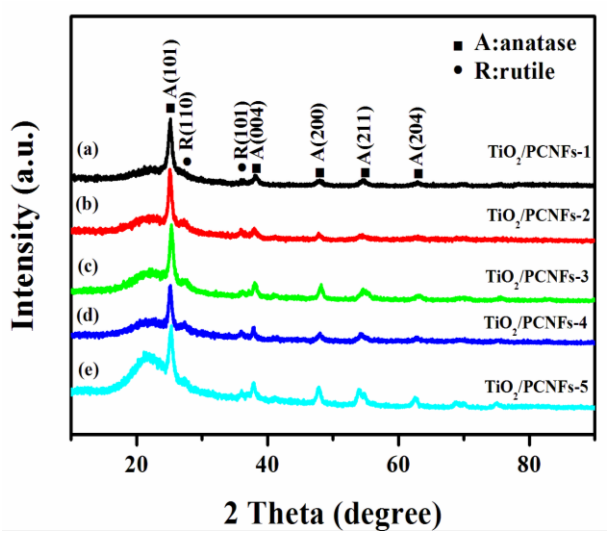

Fig. 3 XRD patterns of the as-fabricated products: (a) TiO_2/PCNFs-1, (b) TiO_2/PCNFs-2, (c) TiO_2/PCNFs-3, (d) TiO_2/PCNFs-4 and (e) TiO_2/PCNFs-5.

3.3. BET, N_2 adsorption-desorption isotherm and BJH pore size studies

In addition, N_2 adsorption/desorption analysis was applied to determine the porous structure of these TiO_2/PCNFs composites. The adsorption/desorption isotherm and the corresponding BJH pore diameter distribution curves of the five samples are presented in Fig. 4. From Fig 4a, with the increase of the pressure, the adsorption amount increases obviously. All the isotherms can be ascribed to type IV isotherms with H4-typehysteresis loops, suggesting the slit pore structure of all samples. From Fig 4b, all samples reveal pore size distribution center at 2-4 nm. The numerous pores

and large surface of PCNFs (1565 m^2/g) are not only favorable for the introduction of TiO_2 into the pore/surface of fibers matrix, but also make the large surface of the heterostructures. The corresponding structural features of these materials are calculated as summarized in Table 1. With the porous structures, all samples show the large surface area about 370, 451, 522, 569 and 442 m^2/g for TiO_2/PCNFs-1, TiO_2/PCNFs-2, TiO_2/PCNFs-3, TiO_2/PCNFs-4 and TiO_2/PCNFs-5, respectively. In addition, compared with pure PCNFs, every TiO_2/PCNFs exhibits the decreased surface area due to the deposition of TiO_2. With the increase of Ti amount, that of TiO_2/PCNFs-4 increases owing to some new surface also being brought from TiO_2 nanorods deposition. However, too much TiO_2 nanorods also decrease the surface area and pore volume of TiO_2/PCNFs-5 (442 m^2/g and 0.188 cm^3/g).

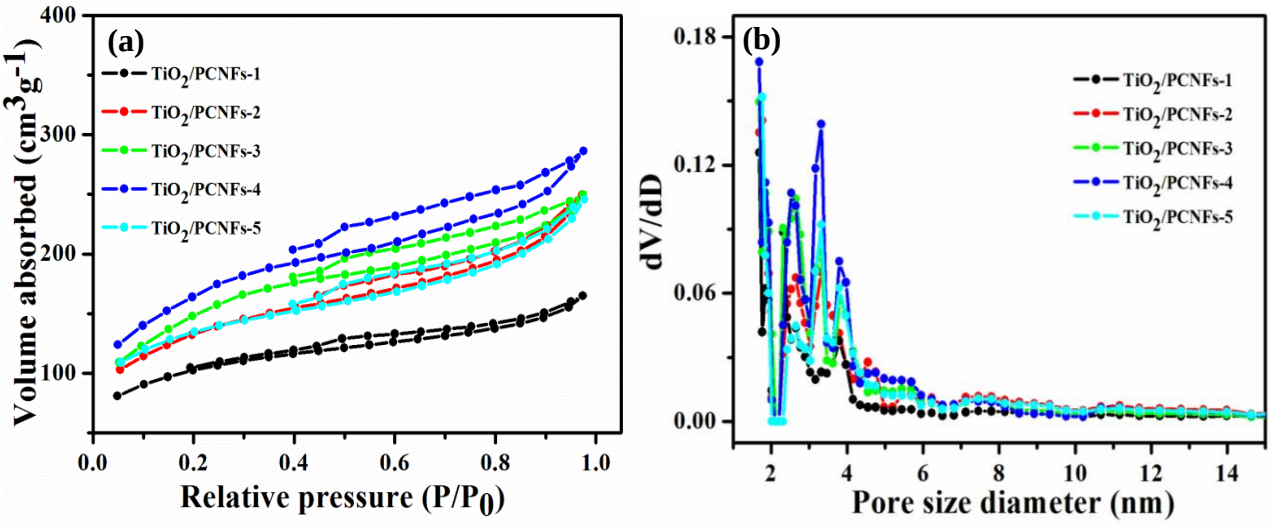

Fig. 4 N_2 adsorption-desorption isotherm (a) and BJH pore size distribution (b) of the five samples.

Table 1 The porous parameters of the samples.

Sample	Surface area (m^2/g)	Pore volume (cm^3/g)	Pore diameter (nm)
TiO_2/PCNFs-1	**370**	**0.099**	**2.65, 3.31, 3.79**
TiO_2/PCNFs-2	**451**	**0.155**	**2.65, 3.32, 3.79**
TiO_2/PCNFs-3	**522**	**0.174**	**2.64, 3.32, 3.79**
TiO_2/PCNFs-4	**569**	**0.185**	**2.53, 3.31, 3.79**
TiO_2/PCNFs-5	**442**	**0.188**	**2.64, 3.31, 3.79**

3.4. UV-Vis absorption spectroscopy studies

The optical properties of the as-synthesized samples have been tested by UV-Vis absorption spectroscopy. As observed in Fig. 5a，the absorption spectra of commercial TiO_2 P25 only exhibits the fundamental absorption band in the UV region due to the wide band gap (3.0 or 3.2 eV). Notably, the curves of TiO_2/PCNFs composites show significant enhanced absorption in visible region. That could be attributed to the following two parts: the carbon is the excellent component to possess full wavelength absorption ability. And the joint electronic system formed from TiO_2 and PCNFs gives rise in synergistic properties.[38]. The bandgap energies estimated from the intercept of the tangents to the plots are 3.14 and 2.2-2.8 eV for the pure TiO_2 and TiO_2/PCNFs

nanocomposite materials, respectively, which is shown in Fig. 5b. The extended absorption in visible region suggests the pretty decolored ability of TiO_2/PCNFs to be used as the photocatalyst under sun light.

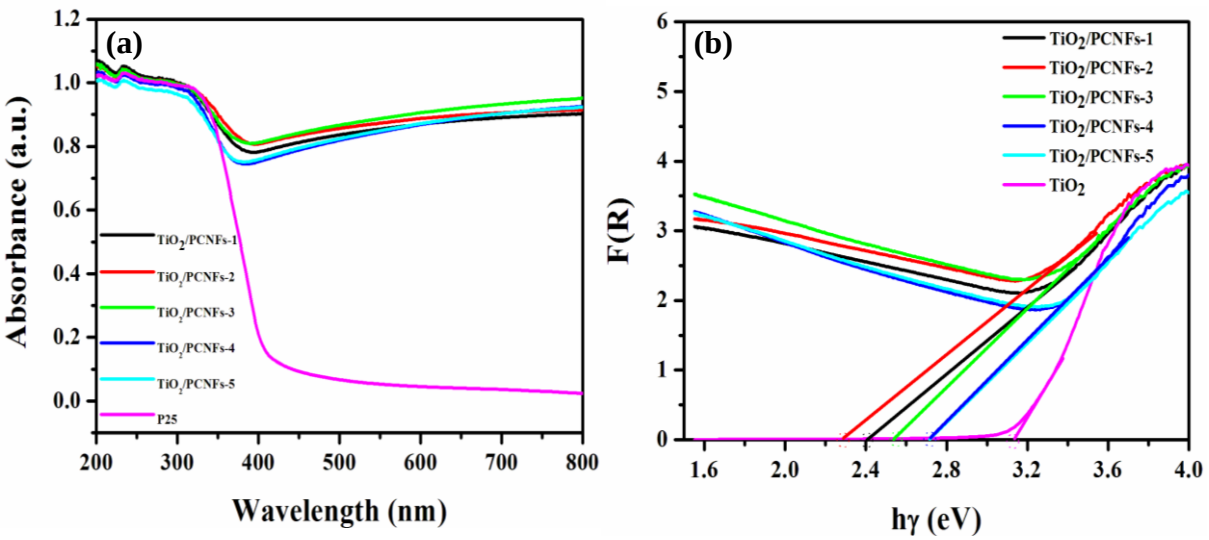

Fig. 5 (a) The UV–Vis absorption spectra of TiO_2/PCNFs-1, TiO_2/PCNFs-2, TiO_2/PCNFs-3, TiO_2/PCNFs-4, TiO_2/PCNFs-5 and P25. (b) The corresponding F(R) versus hγ curves.

3.5. Photocatalytic degradation of dyes studies

To demonstrate the photocatalytic activity of the as-synthesized samples toward organic dye pollutants, these TiO_2/PCNFs heterostructures and P25 were adopted as the catalysts and the photocatalytic degradation tests toward Congo red (CR) were carried out. Fig. 6a-f present the absorption spectra of CR aqueous solution (initial concentration is 10 mg/L) in the presence of the samples under exposure to simulated sun light for different durations. With the increase of the irradiation time, the absorption peak corresponding to CR at 498 nm diminishes gradually, testifying the

degradation of CR. And the degradation rate curves are summarized in Fig. 6g. It takes 170, 170, 130, 50 and 70 min for TiO_2/PCNFs-1, TiO_2/PCNFs-2, TiO_2/PCNFs-3, TiO_2/PCNFs-4 and TiO_2/PCNFs-5 to decolor about 60, 76, 92, 94, and 92 % CR, respectively. TiO_2/PCNFs-4 exhibits the fastest photocatalytic rate owing to the high adsorption capacity (86 %) because of the largest surface area (569 m^2/g). As shown in Fig. 6f, under visible light irradiation for 170 min, merely 27 % of CR is decomposed by using the P25 as the photocatalyst due to the limited visible light utilization.

To further demonstrate the degradation process, the photocatalytic degradation kinetic was also investigated. The linear simulation of degradation of dye concentration can be accounted for by a pseudo first-order model, just so called the Langmuir-Hinshelwood (L-H) model. The L-H model is well established for heterogeneous photocatalysts (at low dye concentration). The relevant equation is as below:

$$r = -dC / dt = k'KC/1 + KC \quad (1)$$

Where r is the rate of dye mineralization, k′ is the rate constant, C is the dye concentration, and K is the adsorption coefficient. By integration, eqn (1) can be arranged into the following:

$$\ln(C/C_0) = -kt \quad (2)$$

Where C_0 is the initial concentration of the dye solution and k is a rate constant. According to eqn (2), rate constant k can be given by the slope of fitting curves, when plotting $\ln(C/C_0)$ against. We are able to find out k from the gradient of the graph of

ln(C/C_0) versus time (t) which is shown in Fig 6h. All samples exhibit the good linear relationship between ln(C/C_0) and irradiation time t. From Fig. 6h, P25 displays the lowest rate constant k = 0.00171 min^{-1} that is because TiO_2 needs UV light to generate photogenerated electron-hole pairs to make sure the photodegradation. After the combination with PCNFs, TiO_2/PCNFs heterostructures possess the enhanced photocatalysis ability owing to the improved absorption in visible light region. TiO_2/PCNFs-1 displays 2 times rate constant (k=0.00381 min^{-1}) more than P25. With the increase of TiO_2, the rate constant increases and TiO_2/PCNFs-4 possesses the highest rate constant k= 0.0158 min^{-1}. Further increasing of TiO_2, the rate constant of TiO_2/PCNFs-5 decreases to k = 0.01193 min^{-1} that is caused by its decreased surface area/pore volume. Moreover, too much TiO_2 nanorods coating outside hinder the light absorption for carbon component and the electron-hole generation as well. The photocatalytic reactivity order is TiO_2/PCNFs-4>TiO_2/PCNFs-3 >TiO_2/PCNFs-5>TiO_2/PCNFs-2>TiO_2/PCNFs-1>P25. Based on the above investigation, then enhanced catalysis efficiency of TiO_2/PCNFs is ascribed to: 1) the improved visible light utilization owing to the synergistic effect of the two components. 2) The enhanced surface area ascribing to the 1D matrix causes the high adsorption capacity due to the tendency of the dyes toward the surface of the catalyst to enhance the degradation.[41, 42]

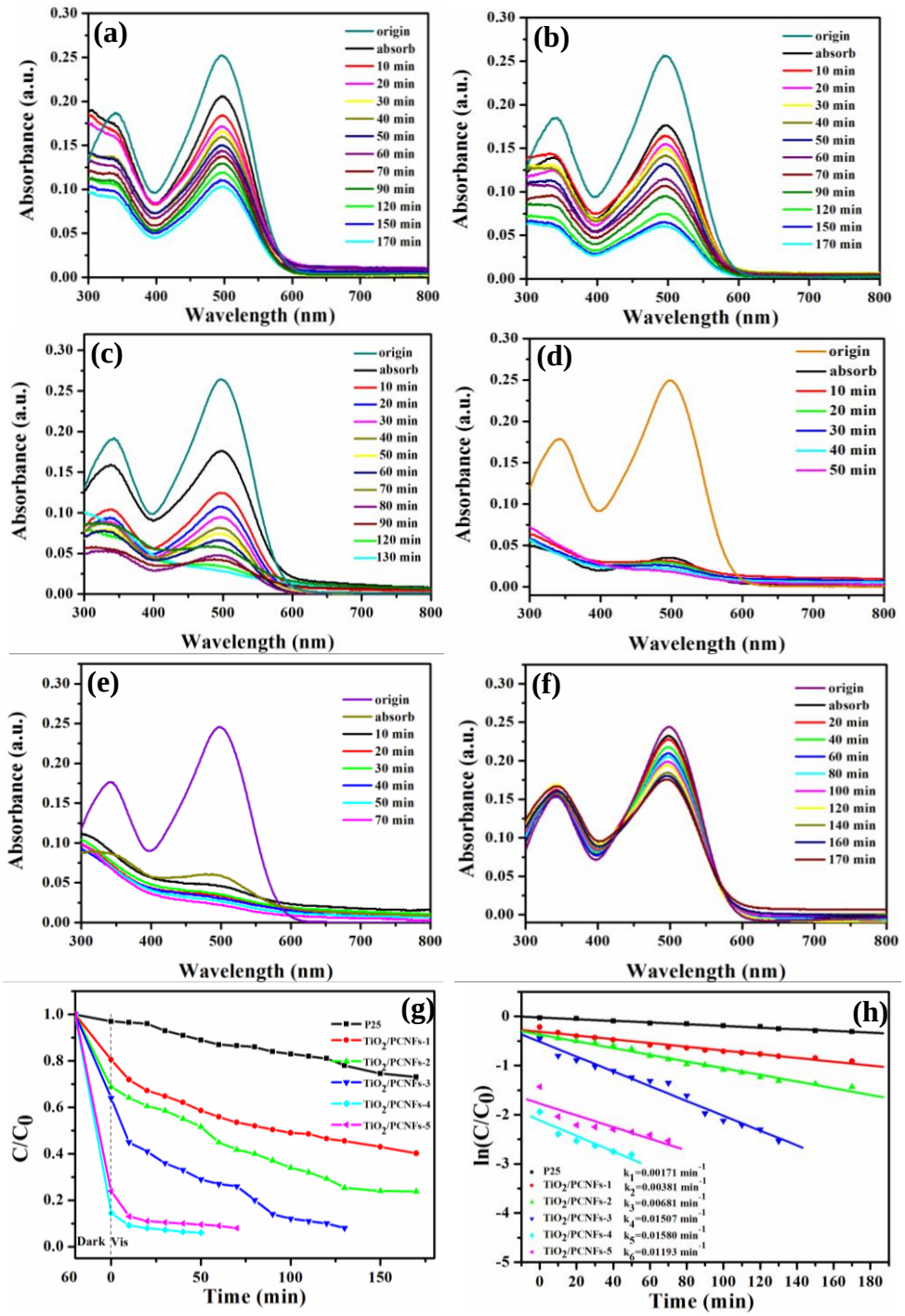

Fig. 6 Absorption spectra of Congo red solution under visible light in the presence of (a) TiO_2/PCNFs-1, (b) TiO_2/PCNFs-2, (c) TiO_2/PCNFs-3, (d) TiO_2/PCNFs-4, (e) TiO_2/PCNFs-5 and (f) P25. (g) Photocatalysis degradation rate of all samples, (h) Kinetic linear simulation curves of Congo red photocatalytic degradation under the visible light.

Considering the good performance of TiO_2/PCNFs-4 on dye treatment, photocatalytic degradation activities of TiO_2/PCNFs-4 heterostructure to methylene blue (MB), methyl orange (MO), eosin red (ER) dyes were also investigated. Fig. 7a-c displays the UV/Vis absorption spectra of dyes in the presence of TiO_2/PCNFs-4 heterostructure under visible light at different time intervals. From Fig. 7a-c, it is clearly seen that the absorption peaks corresponding to dyes diminish gradually with the illumination time prolonged, implying the degradation of dyes. And the photocatalytic activities of TiO_2/PCNFs-4 toward the four dyes are summarized in Fig.7d. As exhibited in Fig. 7d, TiO_2/PCNFs-4 reveals the fastest degradation toward MB, about nearly 100 % decolored efficiency after the dark reaction. In addition, about 95 % MO and 96 % ER is degraded after 20 and 90 min irradiation, respectively. Furthermore, after the dark adsorption, TiO_2/PCNFs-4 reveals about 93, 86, and 32 % adsorption amount to MO, CR, and ER. It is known that, the high adsorption capacity benefits to the photocatalysis due to the enhanced contact between dye molecules and catalyst. Thus it is believed that the fastest degradation to MB can be ascribed to the highest adsorption capacity. Based on the previous reports, the difference of adsorption capacity would be ascribed to the interaction and structure/size matching between the adsorbent and the adsorbate. TiO_2/PCNFs-4 possesses the large surface/pore volume, strong interaction and the well structure matching with typical cationic dyes MB, MO, demonstrating the superior adsorption. Furthermore, for the anionic dyes, the 1D fiber structures always reveal the high adsorption capacity to 1D long-chain dye, and possess the strong electrostatic

interaction with TiO_2/PCNFs-4 (Zeta potential: -5.20±7.25 mV), such as CR, so that TiO_2/PCNFs-4 exhibits the high adsorption ability to CR.[43] However, the decreased adsorption capacity to another anionic dye ER due to the low structure matching between the 2D planar molecular structure of ER and the TiO_2/PCNFs-4 heterostructure (with the slit pore). As shown in Fig. 7d, TiO_2/PCNFs-4 displays the higher adsorption capacitor of MB, MO, and CR than that of ER, but the fast degradation rate of ER also makes 96 % degradation percentage with 90 min irradiation. It is fully proved that the high effective purification ability of TiO_2/PCNFs-4 toward dyes depends on photodegradation rather than the physical adsorption.

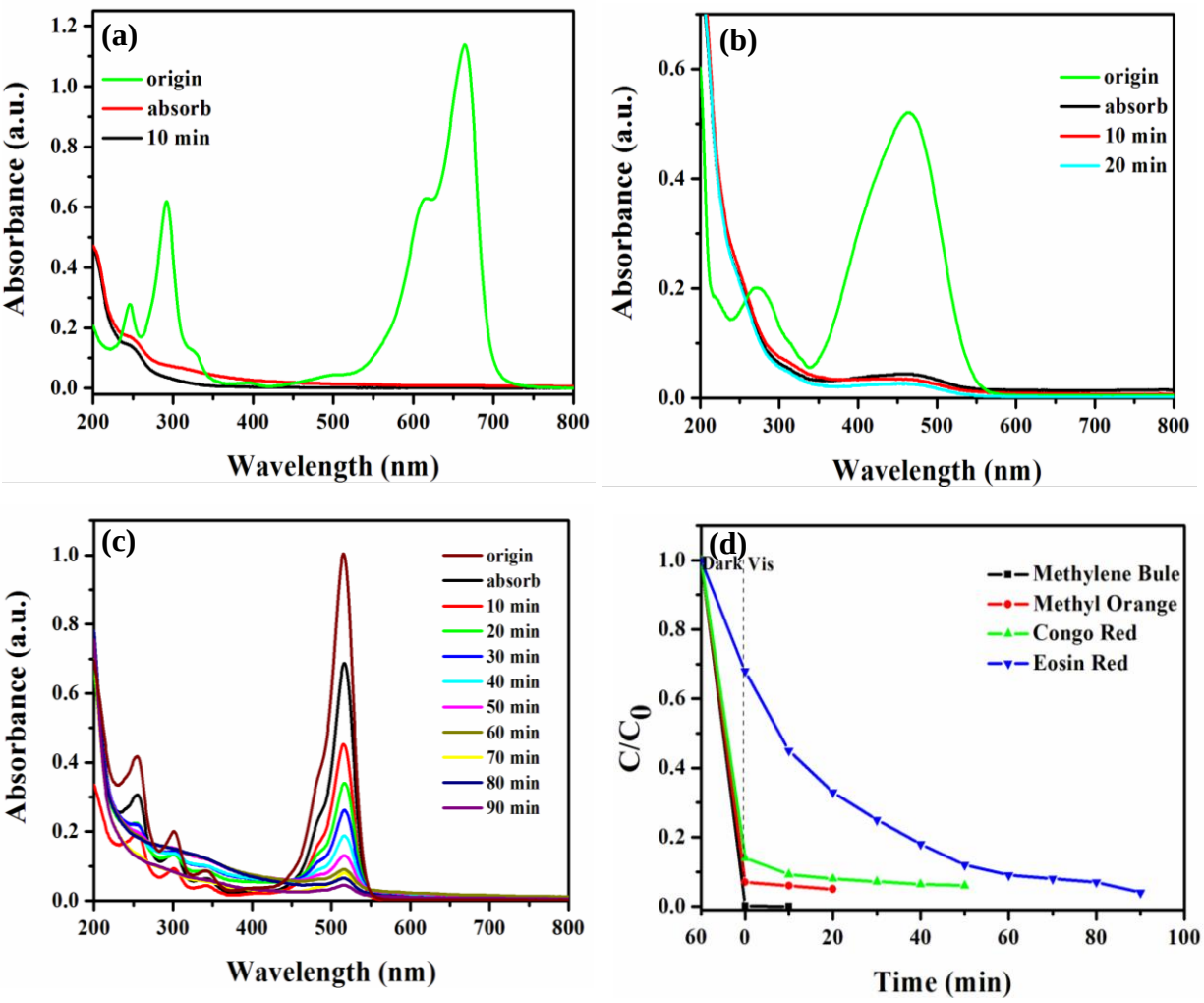

Fig. 7 Variations in adsorption spectra of organic dye solution in the presence of the TiO_2/PCNFs-4 heterostructure irradiated by a visible light for different time periods: (a) methylene blue, (b) methyl orange, (c) eosin red, (d) Photocatalysis degradation rate of all the dyes.

Considering the good photo-degradation of TiO_2/PCNFs-4 toward MB, various MB solutions (20-120 mg/L) were further used to demonstrate the adsorption and degradation activity of TiO_2/PCNFs-4. As shown in Fig. 8b, it costs 20, 40, 70, 70 and 70 min for TiO_2/PCNFs-4 to decompose about 99.5 % (40 mg/L), 99.4%

(60mg/L), 97.0 % (80 mg/L), 89.0 % (100 mg/L) and 75.8 % (120 mg/L) MB, respectively. And the equilibrium adsorption isotherm (dark adsorption) of TiO_2/PCNFs-4 to MB solution was calculated as exhibited in Fig. 8a. With the increase of the dye concentration, the adsorption amount increases dramatically until the adsorption reaches saturation (307.2 mg/g) that is a rather high adsorption amount. Furthermore, as revealed in Fig. 8a, the adsorption isotherm belongs to a type I curve, characteristic of a Langmuir isotherm. And the experimental equilibrium adsorption of dye on the sample was also analyzed by fitting the equilibrium adsorption data using the Langmuir equation:

$$\frac{c_e}{q_e} = \frac{1}{q_m k} + \frac{c_e}{q_m}$$

Where q_m is the theoretical maximum monolayer adsorption capacity (mg/g), k is the Langmuir constant, c_e is equilibrium concentration, and q_e is the equilibrium adsorption amount (mg/g). The corresponding linear Langmuir transform of the isotherm is exhibited in the Fig. 8a inset. From Fig. 8a inset, the adsorption behavior displays a good linear Langmuir relationship with the theoretical maximum adsorption values (q_m = 309.6 mg/g) close to the experimental capacity (307.2 mg/g). The good Langmuir adsorption relationship between MB and TiO_2/PCNFs-4 associated with the high adsorption amount are expected to bring up the enhanced degradation capability.

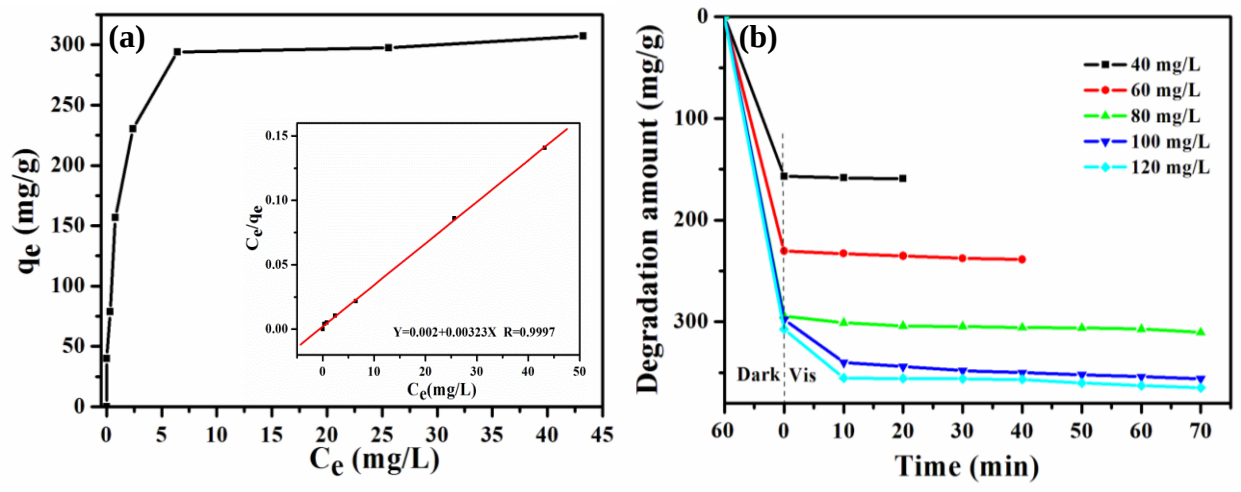

Fig. 8 (a) Effect of the initial dye concentration 10mg/L, 20mg/L, 40mg/L, 60mg/L, 80mg/L, 100mg/L and 120mg/L on the degradation capacity of TiO_2/PCNFs-4 heterostructure, and (b) variation of the degradation capability of the TiO_2/PCNFs-4 (dye/catalyst, mg/g) to degradation time.

To visualize the degradation capability of TiO_2/PCNFs-4 to MB, the variation of the degradation capability (dye/catalyst, mg/g) to degradation time was recorded as displayed in Fig. 8b. TiO_2/PCNFs-4 displays 159.2mg/g degradation capability for 40 mg/L MB under irradiation for 20 min. As increasing the MB concentration to 120 mg/L, the degradation capability increases to 364.8 mg/g after 70 min exposed in simulated sun light. Moreover, the TG-DTA analyses of TiO_2/PCNFs-4 and TiO_2/PCNFs-4 after the treatment of 120 mg/L MB solution for 70 min were carried out. From Fig. 9, the carbon component of TiO_2/PCNFs-4 is about 37.9 % (the weight loss between 200-650 ℃). The residue dye in TiO_2/PCNFs-4 after the photocatalysis

is calculated just about 6.9 % by using the weight loss between 200-650 ℃ minus carbon amount. It further confirms that the high effective purification ability of TiO_2/PCNFs-4 toward MB lies on photodegradation rather than the physical adsorption. The high adsorption capacity benefits the dye molecules to be adsorbed on to the surface of the catalyst to enhance the photocalalysis performance. With the great decoloration capability, TiO_2/PCNFs-4 is expected to possess the potential application on dye adsorption.

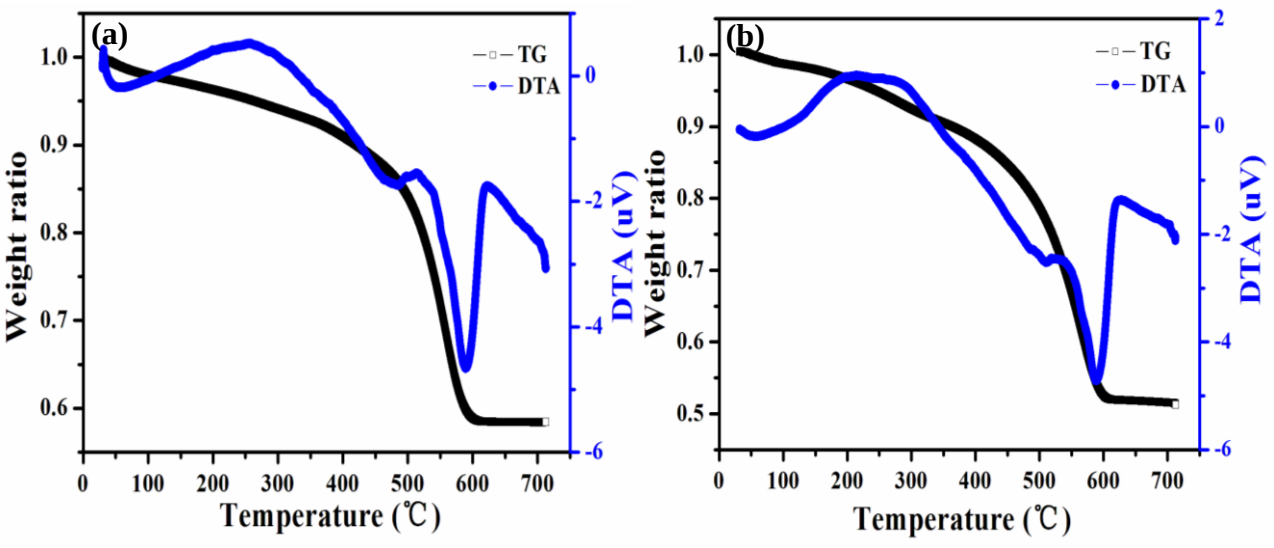

Fig. 9 Thermal gravimetry-differential thermal analysis (TG-DTA) curves of (a) the as-obtained TiO_2/PCNFs-4 heterostructure (b) the TiO_2/PCNFs-4 heterostructure after degradation of 120mg/L MB.

3.6. Photocatalytic mechanism studies

The proposed mechanisms were being discussed to explain the enhancement of the visible light photocatalytic properties of the TiO_2/PCNFs heterostructures (Fig. 10). Firststly, the TiO_2/PCNFs were believed to exhibit cooperative or synergetic effects

between the PCNFs and semiconductive metal oxides. It can be proposed that PCNFs can enhance the photocatalytic activity of TiO_2 in two aspects, namely e^- transportation and adsorption. According to previous reports about the sensitization of TiO_2 by carbon species, the sensitizers are excited by visible-light to generate the charge. The excited charge is then injected into the conduction band of TiO_2. Dissolved oxygen molecules (O_2) reacted with conduction band electrons (e^-) to yield superoxide radical anions (O_2^-), which on protonation generated the hydroperoxy radicals ($HO_2\cdot$), producing hydroxyl radicals ($OH\cdot$), which was a strong oxidizing agent to decompose the organic dye. The relative equations are set out as follow:

$$e^- + O_2 \rightarrow O_2\cdot^-$$
$$O_2\cdot^- + H_2O \rightarrow HO_2\cdot + OH^-$$
$$HO_2\cdot + H_2O \rightarrow H_2O_2 + OH\cdot$$
$$H_2O_2 \rightarrow 2OH\cdot$$
$$OH\cdot + \text{dyes} \rightarrow \text{degraded products}$$

Besides, it is known that many dye molecules also can absorb a certain visible light, so that the contribution of the dye excitation to the photodegradation also should be considered. First, these dye molecules were excited from the ground state (Dye) to the triplet excited state (Dye*) This excited state dye species is further converted into a semi-oxidized radial cation (Dye+) by an electron injection into the conduction band of TiO_2. Due to reaction between these trapped electrons and dissolved oxygen in the system superoxide radical anions ($O_2\cdot^-$) are formed which in turn result into hydroxyl radicals (OH) formation. These OH radicals are mainly responsible for the oxidation of the organic compounds represented by the equations.

$$dye + h\gamma \rightarrow dye^*$$
$$dye^* + TiO_2 \rightarrow dye^+ + TiO_2^-$$

It is believed that the novel heterostructure benefits to enhance the visible light use efficiency and to induce interfacial charge separation and transfer/recycle to make sure the outstanding visible photocatalytic activity.

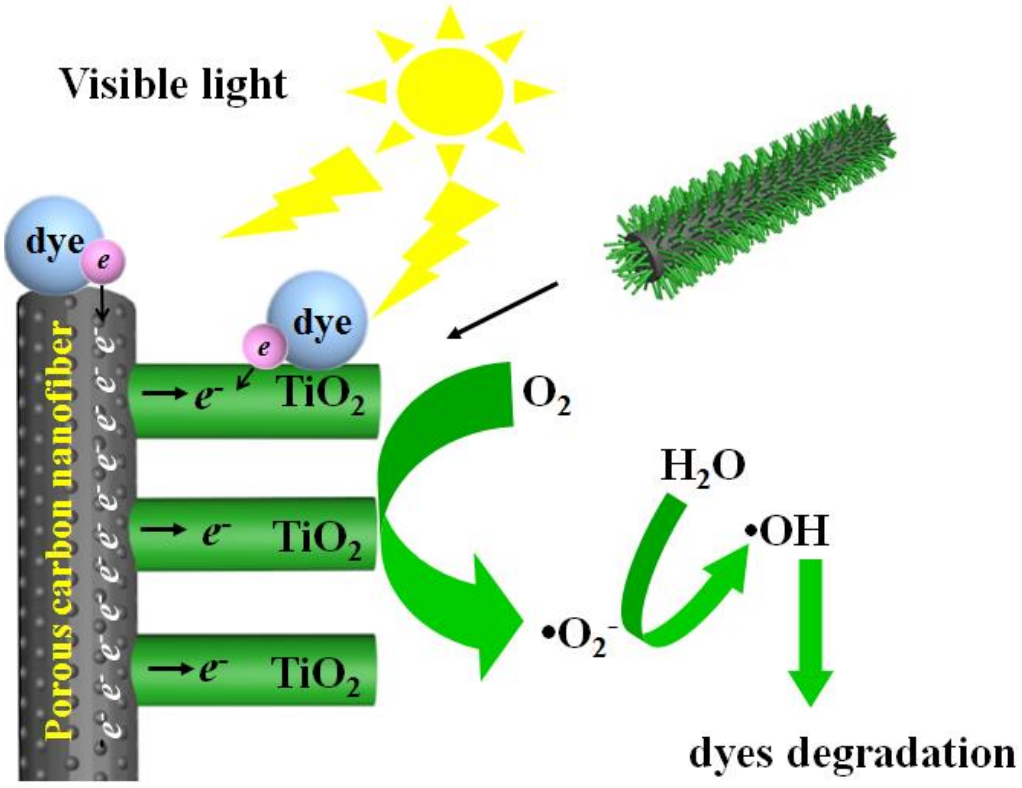

Fig. 10 The schematic of interfacial charge carries generation, transfer, and separation between TiO_2 and porous carbon nanofibers in the TiO_2/PCNFs heterostructure under the visible light.

3.7. Cycle ability studies

Cycling use as well as maintaining high activity of photocatalysts is a critical issue

toward long-term photocatalytic applications. The stability of the as-synthesized TiO_2/PCNFs-4 photocatalyst was evaluated by performing the recycle experiments for degrading MB (10 mg/L) and the results are shown in Fig. 11. After five cycles, it also can decolor about 96 % MB in the pollution solution (10 min). The well recycle ability is significant for catalysts to be used in practical application.

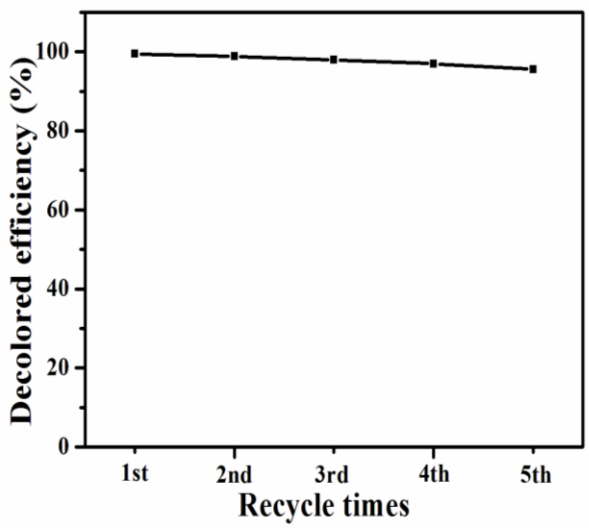

Fig. 11 Cycling tests of photocatalytic activity of the TiO_2/PCNFs-4 heterostructure for MB degradation.

4. Conclusion

In summary, the TiO_2/porous carbon nanofibers heterostructures were successfully fabricated by combining with electrospinning technique and hydrothermal method. Methylene blue, Congo red, methyl orange and eosin red were adopted as the model dyes and the photocatalytic tests were carried out in detail. All nanocomposites exhibit enhanced visible photocatalytic activity that could be ascribed to the improved visible light use efficiency and the separation of photogenerated electrons/holes

derived from the synergetic effect of the two components. On account of the novel porous structure and the appropriate amount of the two components, TiO_2/PCNFs-4 possesses the efficient decolored capacity to methylene blue solution even for the high concentration (120 mg/L). In addition, the high adsorption capacity, lying on surface area of catalysts and structure match between dye molecules and catalysts, helps dye molecules to contact to catalyst and always improves the catalytic sufficiency. That associates with the appropriate amount of every component could be considered for the design and preparation of catalyst.

Acknowledgements

Financial support for this study was provided by the National Natural Science Foundation of China (21471041, 21171045, 21441002), Natural Science Foundation of Heilongjiang Province of China ZD201214.

References

1 M. Wang, J. Ioccozia, L. Sun, C. Lin and Z. Lin, *Energy & Environmental Science*, 2014, **7**, 2182 –2202

2 J. Mu, C. Shao, Z. Guo, M. Zhang, Z. Zhang, P. Zhang, B. Chen and Y. Liu, *Journal of Materials Chemistry*, 2012, **22**, 1786-1793.

3 Y. Tang, P. Wee, Y. Lai, X. Wang, D. Gong, P. D. Kanhere, T. T. Lim, Z. Dong and Z. Chen, *The Journal of Physical Chemistry C*, 2012, **116**, 2772-2780.

4 J. Liao, S. Lin, L. Zhang, N. Pan, X. Cao and J. Li, *ACS Applied Materials & Interfaces*, 2011, **4**, 171-177.

5 W. J. Ong, L. L. Tan, S. P. Chai, S. T. Yong and A. R. Mohamed, *Nanoscale*, 2014, **6**, 1946-2008.

6 W. Zhou, G. Du, P. Hu, G. Li, D. Wang, H. Liu, J. Wang, R. I. Boughton, D. Liu and H. Jiang, *Journal of Materials Chemistry*, 2011, **21**, 7937-7945.

7 K. Lv, B. Cheng, J. Yu and G. Liu, *Physical Chemistry Chemical Physics*, 2012, **14**, 5349-5362.

8 Y. Wang, R. Shi, J. Lin and Y. Zhu, *Energy & Environmental Science*, 2011, **4**, 2922-2929.

9 S. Balachandran and M. Swaminathan, *The Journal of Physical Chemistry C*, 2012, **116**, 26306-26312.

10 M. Muruganandham, R. Amutha, G. J. Lee, S. H. Hsieh, J. J. Wu and M. Sillanp ää, *The Journal of Physical Chemistry C*, 2012, **116**, 12906-12915.

11 J. Huang, G. Tan, H. Ren, W. Yang, C. Xu, C. Zhao and A. Xia, *ACS Applied Materials & Interfaces*, 2014, **6**, 21041-21050.

12 J. Yang, X. Wang, J. Dai and J. Li, *Industrial & Engineering Chemistry Research*, 2014, **53**, 12575-12586.

13 L. P. Zhu, L. L. Wang, N. C. Bing, C. Huang, L. J. Wang and G. H. Liao, *ACS Applied Materials & Interfaces*, 2013, **5**, 12478-12487.

14 G. K. Pradhan, D. K. Padhi and K. M. Parida, *ACS Applied Materials & Interfaces*, 2013, **5**, 9101-9110.

15 S. Bae, S. Kim, S. Lee and W. Choi, *Catalysis Today*, 2014, **224**, 21-28.

16 J. L. Gole, J. D. Stout, C. Burda, Y. Lou and X. Chen, *The Journal of Physical Chemistry B*, 2003, **108**, 1230-1240.

17 R. Ghosh Chaudhuri and S. Paria, *Dalton Transactions*, 2014, **43**, 5526-5534.

18 S. T. Kochuveedu, Y. J. Jang, Y. H. Jang, W. J. Lee, M. A. Cha, H. Shin, S. Yoon, S. S. Lee, S. O. Kim, K. Shin, M. Steinhart and D. H. Kim, *Green Chemistry*, 2011, **13**, 3397-3405.

19 V. Pore, T. Kivela, M. Ritala and M. Leskela, *Dalton Transactions*, 2008, 6467-6474.

20 T. L. Thompson and J. T. Yates, *Chemical Reviews*, 2006, **106**, 4428-4453.

21 X. Guo, W. Di, C. Chen, C. Liu, X. Wang and W. Qin, *Dalton Transactions*, 2014, **43**, 1048-1054.

22 G. Zhou, X. Liu, C. Nan, Y. Liu, D. Wang and X. Chen, *New Journal of Chemistry*, 2013, **37**, 2582-2588.

23 Y. C. Pu, G. Wang, K. D. Chang, Y. Ling, Y. K. Lin, B. C. Fitzmorris, C. M. Liu, X. Lu, Y. Tong, J. Z. Zhang, Y. J. Hsu and Y. Li, *Nano Letters*, 2013, **13**, 3817-3823.

24 X. Zhang, Y. Liu, S. T. Lee, S. Yang and Z. Kang, *Energy & Environmental Science*, 2014, **7**, 1409-1419.

25 A. A. Ismail and D. W. Bahnemann, *Green Chemistry*, 2011, **13**, 428-435.

26 X. Xu, G. Yang, J. Liang, S. Ding, C. Tang, H. Yang, W. Yan, G. Yang and D. Yu, *Journal of Materials Chemistry A*, 2014, **2**, 116-122.

27 S. Dutta, R. Sahoo, C. Ray, S. Sarkar, J. Jana, Y. Negishi and T. Pal, *Dalton*

Transactions, 2015, **44**, 193-201.

28 W. Jia, B. Jia, F. Qu and X. Wu, *Dalton Transactions*, 2013, **42**, 14178-14187.

29 G. W. Cui, W. L. Wang, M. Y. Ma, M. Zhang, X. Y. Xia, F. Y. Han, X. F. Shi, Y. Q. Zhao, Y. B. Dong and B. Tang, *Chemical Communications*, 2013, **49**, 6415-6417.

30 S. Wang, L. Zhao, L. Bai, J. Yan, Q. Jiang and J. Lian, *Journal of Materials Chemistry A*, 2014, **2**, 7439-7445.

31 Z. Zhang, C. Shao, X. Li, Y. Sun, M. Zhang, J. Mu, P. Zhang, Z. Guo and Y. Liu, *Nanoscale*, 2013, **5**, 606-618.

32 D. Zhao, X. Yang, C. Chen and X. Wang, *Journal of Colloid and Interface Science*, 2013, **398**, 234-239.

33 P. Song, X. Zhang, M. Sun, X. Cui and Y. Lin, *Nanoscale*, 2012, **4**, 1800-1804.

34 S. Liu, C. Liu, W. Wang, B. Cheng and J. Yu, *Nanoscale*, 2012, **4**, 3193-3200.

35 W. Gao, M. Wang, C. Ran and L. Li, *Chemical Communications*, 2015, **51**, 1709-1712.

36 X. Wang, K. Zhang, X. Guo, G. Shen and J. Xiang, *New Journal of Chemistry*, 2014, **38**, 6139-6146.

37 J. Zhuang, Q. Tian, H. Zhou, Q. Liu, P. Liu and H. Zhong, *Journal of Materials Chemistry*, 2012, **22**, 7036-7042.

38 P. Zhang, C. Shao, Z. Zhang, M. Zhang, J. Mu, Z. Guo and Y. Liu, *Nanoscale*, 2011, **3**, 2943-2949.

39 Y. Meng, D. Gu, F. Zhang, Y. Shi, L. Cheng, D. Feng, Z. Wu, Z. Chen, Y. Wan, A. Stein and D. Zhao, *Chemistry of Materials*, 2006, **18**, 4447-4464.

40 Y. Cao, T. He, Y. Chen and Y. Cao, *J. Phys. Chem. C*, 2010, **114**, 3627.

41 S. Ma, J. Xue, Y. Zhou, Z. Zhang and X. Wu, *CrystEngComm*, 2014, **16**, 4478-4484.

42 H. Y. Jing, T. Wen, C. M. Fan, G. Q. Gao, S. L. Zhong and A. W. Xu, *Journal of Materials Chemistry A*, 2014, **2**, 14563-14570.

43 Y. Dong, H. Lin, Q. Jin, L. Li, D. Wang, D. Zhou and F. Qu, *Journal of Materials Chemistry A*, 2013, **1**, 7391-7398.